Improved Visualization of Juxtaprosthetic Tissue Using Metal Artifact Reduction Magnetic Resonance Imaging: Experimental and Clinical Optimization of Compressed Sensing SEMAC

Jungmann, Pia M ; Bensler, Susanne ; Zingg, Patrick ; Fritz, Benjamin ; Pfirrmann, Christian W ; Sutter, Reto

Abstract: OBJECTIVES The purpose of this study was to identify an optimal imaging protocol for metal artifact reduced magnetic resonance imaging by application of different imaging and postprocessing parameters in compressed sensing slice-encoding for metal artifact correction (CS-SEMAC) and to test it in patients with total hip arthroplasty (THA). MATERIALS AND METHODS In an experimental setup, a phantom consisting of a standard THA embedded in gadolinium-containing agarose was scanned at 1.5 T. Pulse sequences included coronal short tau inversion recovery (STIR), T1-weighted (w), and T2-w CS-SEMAC sequences. All pulse sequences were acquired with 11, 19, and 27 slice-encoding steps (SESs), respectively. For each raw dataset, postprocessing was performed with variations of the parameters: (1) number of iterations (5, 10, 20, 30, 50) and (2) normalization factor (0.0005, 0.001, 0.002, 0.003, 0.005). Following, in clinical magnetic resonance scans of patients with THA, identical STIR, T1-w, and T2-w pulse sequences with 11 and 19 SESs were acquired and were postprocessed similarly with variations in parameters. Semiquantitative outcome measures were assessed on a 5-point scale (1 = best, 5 = worst). The overall best image quality was determined. Signal-to-noise ratio and contrast-to-noise ratio were calculated. Statistical analyses included descriptive statistics, t-tests, multivariate regression models, and partial Spearman correlations. RESULTS Scan times varied between 2:24 (T2-w, 11 SESs) and 8:49 minutes (STIR, 27 SESs). Reconstruction times varied between 3:14 minutes (T1-w, 11 SESs, 5 iterations) and 85:00 minutes (T2-w, 27 SESs, 50 iterations). Signal-to-noise ratio and contrast-to-noise ratio increased with increasing SESs, iterations, and normalization factor. In phantom scans, artifact reduction was optimal with an intermediate normalization factor (0.001) and improved with higher SESs and iterations. However, iterations greater than 20 did not improve artifact reduction or image quality further. On the contrary, ripple artifacts increased with higher SESs and iterations. In clinical scans, up to 20 iterations reduced blurring of the image; no further reduction was observed with iterations greater than 20. A normalization factor of 0.001 or 0.002 was best for reduction of blurring, whereas the soft tissue contrast was better and the distortion of soft tissue was less severe with lower normalization factors. Overall best soft tissue image quality was found for STIR and T1-w images with 19 SESs, 10 iterations, and a normalization factor of 0.001, and for T2-w images with 11 SESs, 10 iterations, and a normalization factor of 0.0005. CONCLUSIONS Optimized advanced acceleration and reconstruction algorithms of CS-SEMAC have been identified to reduce metal artifacts in patients with THA enabling imaging with clinically feasible acquisition and reconstruction times.

DOI: https://doi.org/10.1097/RLI.0000000000000504

Journal Article
Published Version

Originally published at:
Jungmann, Pia M; Bensler, Susanne; Zingg, Patrick; Fritz, Benjamin; Pfirrmann, Christian W; Sutter, Reto (2019). Improved Visualization of Juxtaprosthetic Tissue Using Metal Artifact Reduction Magnetic Resonance Imaging: Experimental and Clinical Optimization of Compressed Sensing SEMAC. Investigative Radiology, 54(1):23-31.
DOI: https://doi.org/10.1097/RLI.0000000000000504

Improved Visualization of Juxtaprosthetic Tissue Using Metal Artifact Reduction Magnetic Resonance Imaging

Experimental and Clinical Optimization of Compressed Sensing SEMAC

Pia M. Jungmann, MD,† Susanne Bensler, MD,*‡ Patrick Zingg, MD,§ Benjamin Fritz, MD,* Christian W. Pfirrmann, MD,* and Reto Sutter, MD**

Abstract: Objectives: The purpose of this study was to identify an optimal imaging protocol for metal artifact reduced magnetic resonance imaging by application of different imaging and postprocessing parameters in compressed sensing slice-encoding for metal artifact correction (CS-SEMAC) and to test it in patients with total hip arthroplasty (THA).

Materials and Methods: In an experimental setup, a phantom consisting of a standard THA embedded in gadolinium-containing agarose was scanned at 1.5 T. Pulse sequences included coronal short tau inversion recovery (STIR), T1-weighted (w), and T2-w CS-SEMAC sequences. All pulse sequences were acquired with 11, 19, and 27 slice-encoding steps (SESs), respectively. For each raw dataset, postprocessing was performed with variations of the parameters: (1) number of iterations (5, 10, 20, 30, 50) and (2) normalization factor (0.0005, 0.001, 0.002, 0.003, 0.005). Following, in clinical magnetic resonance scans of patients with THA, identical STIR, T1-w, and T2-w pulse sequences with 11 and 19 SESs were acquired and were postprocessed similarly with variations in parameters. Semiquantitative outcome measures were assessed on a 5-point scale (1 = best, 5 = worst). The overall best image quality was determined. Signal-to-noise ratio and contrast-to-noise ratio were calculated. Statistical analyses included descriptive statistics, *t*-tests, multivariate regression models, and partial Spearman correlations.

Results: Scan times varied between 2:24 (T2-w, 11 SESs) and 8:49 minutes (STIR, 27 SESs). Reconstruction times varied between 3:14 minutes (T1-w, 11 SESs, 5 iterations) and 85:00 minutes (T2-w, 27 SESs, 50 iterations). Signal-to-noise ratio and contrast-to-noise ratio increased with increasing SESs, iterations, and normalization factor. In phantom scans, artifact reduction was optimal with an intermediate normalization factor (0.001) and improved with higher SESs and iterations. However, iterations greater than 20 did not improve artifact reduction or image quality further. On the contrary, ripple artifacts increased with higher SESs and iterations. In clinical scans, up to 20 iterations reduced blurring of the image; no further reduction was observed with iterations greater than 20. A normalization factor of 0.001 or 0.002 was best for reduction of blurring, whereas the soft tissue contrast was better and the distortion of soft tissue was less severe with lower normalization factors. Overall best soft tissue image quality was found for STIR and T1-w images with 19 SESs, 10 iterations, and a normalization factor of 0.001, and for T2-w images with 11 SESs, 10 iterations, and a normalization factor of 0.0005.

Conclusions: Optimized advanced acceleration and reconstruction algorithms of CS-SEMAC have been identified to reduce metal artifacts in patients with THA enabling imaging with clinically feasible acquisition and reconstruction times.

Received for publication April 22, 2018; and accepted for publication, after revision, June 28, 2018.

From the *Department of Radiology, Balgrist University Hospital, †Department of Neuroradiology, University Hospital Zurich, University of Zurich, Zurich; ‡Institute of Radiology, Kantonsspital Baden, Baden; and §Department of Orthopedic Surgery, Balgrist University Hospital, University of Zurich, Zurich, Switzerland.

Conflicts of interest and sources of funding: none declared.

Correspondence to: Pia M. Jungmann, MD, Department of Neuroradiology, University Hospital of Zurich, University of Zurich, Frauenklinikstrasse 10, 8091 Zurich, Switzerland. E-mail: pia.jungmann@usz.ch.

Supplemental digital contents are available for this article. Direct URL citations appear in the printed text and are provided in the HTML and PDF versions of this article on the journal's Web site (www.investigativeradiology.com).

ISSN: 0020-9996/18/0000–0000
DOI: 10.1097/RLI.0000000000000504

Key Words: magnetic resonance imaging, artifacts, implants, experimental

(*Invest Radiol* 2018;00: 00–00)

Because of a rapidly growing number of patients with metal implants, metal artifact reduction magnetic resonance sequences (MARSs) are increasingly important in clinical practice.[1–4] Besides conventional high bandwidth MARS imaging, dedicated techniques such as slice-encoding for metal artifact correction (SEMAC) were developed.[5,6] The efficacy of SEMAC with respect to excellent correction of in-plane artifacts and through-plane artifacts was confirmed for different joint replacements. An improved diagnostic quality with clinical relevance was demonstrated.[7–9] Despite, the major drawback of the SEMAC technique remained its prolonged scan time, that may reach about 10–15 minutes, compared to 4–5 minutes for a high bandwidth conventional MARS scan.[7,10]

To reduce scanning times, complex advanced image reconstruction algorithms have been implemented in postprocessing algorithms.[11] Along with partial Fourier, undersampling and parallel imaging these algorithms have been combined with SEMAC techniques.[1] Compressed sensing SEMAC (CS-SEMAC) techniques use sparsity-driven and CS-based k-space undersampled SEMAC data with iterative reconstruction.[12–16] New CS-SEMAC techniques aim to decrease artifacts, increase image resolution, optimize image quality, and most importantly reduce scan time in comparison to standard SEMAC techniques. It was demonstrated that CS-SEMAC sequences are applicable in clinically feasible scan times of less than 5 minutes equivalent to those of high bandwidth conventional MARS sequences.[10] At the same time, CS-SEMAC sequences provide a potent artifact reduction similar to lengthier SEMAC sequences for hip, knee, and ankle arthroplasties.[10,13,17] However, the optimal CS-SEMAC protocol still needs to be defined to allow for improved evaluation of juxtaprosthetic tissue.

Main CS-SEMAC parameters that can be modified are slice-encoding steps (SESs), number of iterations, and the normalization factor, also known as "regularization parameter". The SESs are the number of adjacent slices whose signal is assessed for artifact reduction during readout for one specific slice.[5] Iterations are additional correction algorithms that reduce reconstruction artifacts and improve image clarity. Higher normalization factors are applied to decrease the image noise. The scan times increase with higher numbers of SESs. The reconstruction times at postprocessing increase with higher number of SESs, iterations, and normalization factors.

To the best of our knowledge, there has not been a systematic evaluation of the best imaging parameters. Previous literature reported the use of an SES factor of 19, iterations ranging from 20 to 30 and normalization factors ranging from 0.0025 to 0.008.[10,13] We hypothesized that imaging parameters as previously published might be sufficient for clinical use, but that image quality could be further improved using higher SESs and normalization factors.

The purpose of this study was to identify an optimal imaging protocol for metal artifact reduced magnetic resonance imaging (MRI) by application of different imaging and postprocessing parameters in

compressed sensing slice-encoding for metal artifact correction (CS-SEMAC) and to test it in patients with total hip arthroplasty (THA).

MATERIALS AND METHODS

The study was reviewed and approved by the local institutional review boards. The study was performed with informed consent and has been conducted according to the Declaration of Helsinki with written informed patient consent. In this study, an experimental phantom was used to evaluate a range of different CS-SEMAC parameters for their efficacy regarding metal artifact reduction. Second, the juxtaprosthetic soft tissue MRI scan quality was assessed patients with THA undergoing MRI of the hip for clinical indications using the best CS-SEMAC parameters as derived from the phantom experiment.

Experimental Setup

A phantom was constructed by embedding a standard total hip replacement (titanium Quadra-H stem, titanium Versafit-CC cup, femoral head replacement with cobalt-28 chromium-6 molybdenum alloy casting; Medacta, Castel San Pietro, Switzerland) and polypropylene structures in agarose 2% containing gadolinium (Gadovist 1.0; 0.1 mmol/L).[18] The mixture surrounded the implant 20 mm or more in every direction.

Patients

After the feasibility of the pulse sequences was confirmed in phantom scans, each CS-SEMAC pulse sequence was evaluated in 1 patient, respectively, with a total number of 3 patients: These clinical scans were then used to perform a number of reconstructions with variations in parameters (25 reconstructions per pulse sequence and per number of SESs), as described in the postprocessing section. The patients were consecutive patients with THA who received MARS imaging of the hip due to clinical complaints. The STIR images were acquired to assess the integrity of the gluteal muscles in a 78-year-old female patient with a THA of the right hip. The T1-weighted (w) images were acquired to exclude loosening and pseudotumor formation in a 71-year-old female patient with a THA of the right hip. The T2-w images were acquired in a 57-year-old female patient with a THA of the right hip due to pain in the trochanteric region and to exclude loosening of the THA. Patients were included if they had received a THA and were referred for an MRI of the hip for clinical indications at our institution. Exclusion criteria were contraindications to MRI, or the presence of a revision THA. No patients had to be excluded.

Magnetic Resonance Imaging

Magnetic resonance imaging was performed at a 1.5 T scanner (Magnetom Avanto; Siemens Healthcare, Erlangen, Germany) using a 6-channel body phased array coil anteriorly and 2 spine coil clusters (3 channels each) posteriorly. A work-in-progress software package that included the postprocessing algorithm of compressed sensing and SEMAC techniques was provided by Siemens Healthcare. Coronal STIR images (repetition time [TR], 4570 milliseconds; echo time [TE], 36 milliseconds; inversion time, 160 milliseconds; refocusing flip angle, 140 degrees; pixel size, 1.2 × 1.2 mm; field of view [FOV], 300 mm; slices, 29; slice thickness, 4 mm; gap 0 mm; bandwidth, 501 Hz/pixel; turbo factor, 9; view angle tilting [VAT], 100; phase encoding direction, R>>L; SESs, 11, 19, and 27; acquisition time, 4:15, 6:30, and 8:49 minutes, respectively), T2-w turbo spin echo images (TR, 5270 milliseconds; TE, 86 milliseconds; refocusing flip angle, 146; pixel size, 0.8 × 0.8 mm; FOV, 243 mm; slices, 27; slice thickness, 4mm; gap 0 mm; bandwidth, 504 Hz/pixel; turbo factor, 23; VAT, 100; phase encoding direction, R>>L; SESs, 11, 19, and 27; acquisition time, 2:24, 3:43, and 5:02 minutes), and T1-w turbo spin echo images (TR, 449 milliseconds; TE, 8.5 milliseconds; refocusing flip angle, 180; pixel size, 0.8 × 0.8 mm; FOV, 270 mm; slices, 27; slice thickness, 3.5mm; gap 0 mm; bandwidth, 504 Hz/pixel; turbo factor, 9; VAT, 100; phase encoding direction, R>>L; SESs, 11, 19, and 27; acquisition time, 3:10, 5:03, and 6:51 minutes) were acquired. The MRI scans of the phantom were acquired using SESs of 11, 19, and 27. In addition, MRI scans were acquired in patients with THA using 11 and 19 SESs.

Postprocessing

Postprocessing was performed at the console of the MR scanner. The number of iterations and the normalization factor (regularization parameter) used for image reconstruction were varied, both for the phantom scans and for the clinical scans. The numbers of iterations applied were 5, 10, 20, 30, and 50, which were all individually combined with a normalization factor of 0.0005, 0.001, 0.002, 0.003, and 0.005 resulting in 25 image datasets for each raw data acquisition.

Semiquantitative Assessment of MRI Scans

All MRI datasets were transferred on Picture Archiving Communication System (PACS) workstations (Easy Vision; Philips, Best, the Netherlands) and were evaluated semiquantitatively by 2 readers in consensus (P.M.J., S.B.; 10 and 13 years of experience, respectively). Outcome measures were assessed on a 5-point scale (1 = best, 5 = worst). Artifact reduction was scored on phantom images by use of the parameters "in-plane distortion," "through-plane distortion," "ripple artifacts," and "overall artifacts." In-plane distortion was defined as signal displacement within 1 plane. Through-plane distortion was defined as signal displacement to adjacent planes.[9] Ripple artifacts were previously described as typical for SEMAC sequences.[19] They appear as multiple rings of signal loss and signal pile-up in-plane adjacent to round contours of the implant (Fig. 1A). Soft tissue image quality was scored on clinical images of patients by use of the parameters "blurring," "soft tissue contrast," "distortion of soft tissue," "ripple artifacts," and "overall image quality." The best image dataset of each iteration group and the best image dataset of each normalization group were chosen, finally resulting in a best image for each SESs group and an overall best image for each pulse sequence.

Signal-to-Noise Ratio and Contrast-to-Noise Ratio Measurements

To calculate signal-to-noise ratio (SNR) and contrast-to-noise ratio (CNR) regions of interest (ROIs) were drawn manually on MRI scans (round ROIs, identical area of 100 mm^2 for all ROIs) using OsiriX Lite 7.0.2 software (Pixmeo; Bernex, Switzerland). On phantom images, ROIs were placed on room air and on the agarose/gadolinium mixture ($SI_{agarose}$). On clinical images, ROIS were placed on room air, on muscle tissue (adductor muscles; SI_{muscle}), on subcutaneous fat (SI_{fat}), and on the bladder (SI_{fluid}). ROIs and ROI placements were identical for each image data reconstruction to avoid measurement bias. $SD_{background}$ was defined as the first positive standard deviation (SD) of the signal intensity of the room air. SI_{ROI} was defined as the mean signal intensity (SI) of the respective tissue. SNR_{ROI} was calculated as $SNR_{ROI} = 0.655 \times SI_{ROI}/SD_{background}$.[20] CNR was calculated as the difference of SNR between 2 tissues of interest ($SNR_{ROI\ 1} - SNR_{ROI\ 2}$). All measurements were performed by one reader (P.M.J.; 10 years of experience).

Statistical Analysis

Statistical processing was performed with SPSS version 20.0 (IBM Corp, Armonk, NY) and Microsoft Excel for Mac Version 2017 15.40 (Microsoft Corporation, Redmond, WA) (P.M.J.). Results are reported as mean ± standard deviation (SD) if not stated otherwise. Mean differences between groups ± standard error of the mean (SEM) and 95% confidence intervals (95% CIs, lower value, upper value) were determined. Differences between groups were assessed via independent

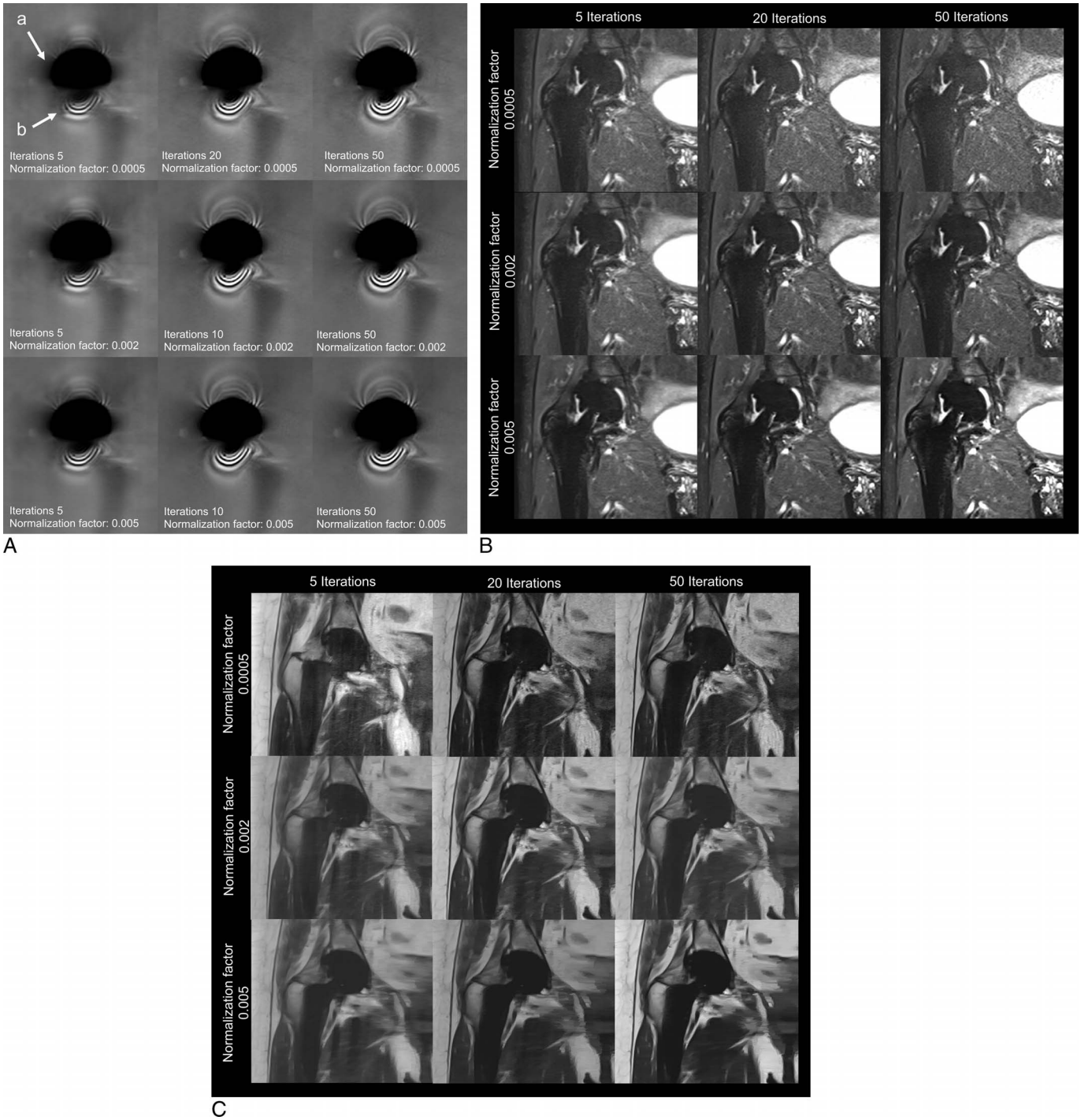

FIGURE 1. Overview of variations of pulse sequence parameters in a phantom and in patients. Images are given exemplarily for all combinations of 5, 20, and 50 iterations with normalization factors of 0.0005, 0.002, and 0.005. A, Artifacts on coronal short tau inversion recovery (STIR) CS-SEMAC phantom scans with 11 slice-encoding steps. Minor in-plane distortion (A) is depicted on the image with 5 iterations and a normalization factor of 0.0005 (upper left). Ripple artifacts (B) worsened with increasing numbers of iterations (from left to right). B, Clinical STIR CS-SEMAC scans with 19 slice-encoding steps in a patient with THA of the right hip. Besides other quality parameters, on STIR sequences blurring may be depicted particularly in case of a normalization factor of 0.0005 (1B first row). C, Clinical T2-weighted CS-SEMAC scans with 11 slice-encoding steps in a patient with THA of the right hip. On T2-weighted sequences distortion of soft tissue may be depicted around the bladder particularly in case of high normalization factors (1C bottom row). With more iterations and higher normalization factors, the image appearance becomes artificial.

samples *t*-tests. Multivariate regression models were used to determine independent influence factors for each assessed artifact and image quality parameter. Partial Spearman correlations (controlling for pulse sequences) were calculated to assess correlations of SNR and CNR with SESs, iterations, and normalization factors. All tests were performed based on a 0.05 level of significance.

RESULTS

Image Acquisition and Reconstruction

Image acquisition and reconstruction was feasible. However, during the acquisition of T1-w and T2-w CS-SEMAC images of the phantom with the maximum number of 27 SESs, the MR console crashed several times. Similarly, during postprocessing and image reconstruction of CS-SEMAC data with 27 SESs, the systems went down several times. Scanning and reconstruction of CS-SEMAC data with 11 and 19 SESs was performed without complications. Because of these technical issues during the phantom scans, clinical images in the patients were acquired with 11 and 19 SESs only.

All scans had a clinically feasible acquisition time. The acquisition time was 4:15 to 8:49 minutes for STIR sequences, 3:10 to 6:51 minutes for T1-w sequences, and 2:24 to 5:02 minutes for T2-w sequences with increasing acquisition times for increasing numbers of SESs.

The time for reconstruction of the image datasets varied between 3:14 minutes (T1-w, 11 SESs, 5 iterations) and 85:00 minutes (T2-w, 27 SESs, 50 iterations). For CS-SEMAC sequences with 19 SESs, the reconstruction time was 5:40 to 32:21 minutes for STIR sequences, 4:13 to 30:30 minutes for T1-w sequences, and 5:53 to 46:48 minutes for T2-w sequences with longer reconstruction times for increasing numbers of iterations.

Semiquantitative Assessment of MRI Scans

Experimental Phantom Scans

Good artifact reduction was achieved for all images and artifacts varied only slightly (Supplementary Material S1, Supplemental Digital Content 1, http://links.lww.com/RLI/A395). There were no through-plane artifacts detected on any of the reconstructed images (mean score ± SD, 1 ± 0). Ripple artifacts were less severe on T1-w images than on STIR images ($P = 0.025$). In-plane distortion and overall artifacts were significantly less on T1-w images than on T2-w or STIR images ($P < 0.001$).

Ripple artifacts increased with increasing numbers of SESs (Table 1) and with more iterations, whereas they were unaffected by the normalization factor (Table 2, Figs. 1A and 2). The least ripple artifacts were found on T1-w images with 11 SESs and 5 iterations. In-plane distortion was reduced with increasing numbers of SESs and with more iterations. Although in-plane distortion was reduced with 20 iterations as compared with 5 ($P < 0.001$) or 10 ($P = 0.004$) iterations, no further improvement was observed with application of 30 or 50 iterations ($P > 0.05$). Application of a normalization factor of 0.005 increased in-plane distortion significantly as compared with a normalization factor of 0.002 ($P = 0.011$). Scores for overall artifacts improved significantly with application of 19 SESs instead of 11 SESs ($P < 0.001$), whereas there was no further improvement with application of 27 SESs ($P = 0.678$). Similarly, scores for overall artifacts improved significantly with application of 10 iterations instead of 5 iterations ($P = 0.003$) and with application of 20 instead of 10 iterations ($P < 0.001$), but there was no further improvement with application of 30 or 50 SESs ($P > 0.05$). Overall artifacts were less severe with application of low normalization factors (0.0005, 0.001, or 0.002) than with application of higher normalization factors (0.002 vs 0.005, $P < 0.001$).

In multivariate regression analyses, SESs ($\beta = 0.324$; $P < 0.001$) and iterations ($\beta = 0.695$, $P < 0.001$) were identified to influence ripple artifacts significantly and independently. All parameters were identified to influence in-plane distortion significantly: pulse sequence ($\beta = 0.118$, $P = 0.011$), SESs ($\beta = -0.528$, $P < 0.001$), iterations ($\beta = -0.435$, $P < 0.001$), and normalization factor ($\beta = 0.243$, $P < 0.001$). SESs ($\beta = -0.405$, $P < 0.001$), iterations ($\beta = -0.524$, $P < 0.001$), and normalization factor ($\beta = 0.264$, $P < 0.001$) were identified to influence overall artifacts significantly.

Overall best artifact reduction was found for all pulse sequences with 19 SESs and 20 iterations. The optimum normalization factor was 0.002 for STIR and T2-w sequences and 0.001 for T1-w sequences.

Clinical Scans

Of note, in clinical scans, no ripple artifacts could be detected. There was significantly less blurring on T2-w images than on STIR or T1-w images ($P = 0.014$ and $P < 0.001$; Table 1). Soft tissue contrast, distortion of soft tissue, and overall image quality were significantly better for STIR images than for T1-w and T2-w images (all $P < 0.001$), whereas there was no significant difference between T1-w and T2-w images ($P > 0.005$).

Regarding the soft tissue image quality, blurring did not differ between 11 and 19 SESs and decreased from 5 to 10 ($P = 0.046$) and 20 iterations ($P < 0.001$); more iterations (30 or 50) did not decrease blurring further (Table 2, Supplementary Material S2, Supplemental Digital Content 2, http://links.lww.com/RLI/A396). A normalization factor of 0.001 resulted in least blurring. Blurring can most easily be depicted on STIR images (Fig. 1B). Soft tissue contrast improved with 19 SESs as compared with 11 SESs ($P < 0.001$). While iterations did not have a significant influence on soft tissue contrast, smaller normalization factors were beneficial for soft tissue contrast. Soft tissue contrast may best be evaluated when considering the muscle fiber delineation, which disappears with high normalization factors in particular on T2-w images (Fig. 1C). Distortion of soft tissues was observed less on images with 19 SESs than with 11 SESs ($P = 0.034$). Least soft tissue distortion was detected for 20 iterations, and more severe soft tissue distortion was observed with fewer or more iterations. However, the difference was not significant (5 vs 20, $P = 0.080$; 20 vs 50, $P = 0.234$). Distortion was distinctly worse with increasing normalization factors of 0.002 and higher (0.001 vs 0.002, $P < 0.001$), and the images appeared more and more like artificial drawings (pastel-like), particularly on T1-w and T2-w images. Although overall image quality was scored best for 19 SESs and 10 iterations, it did not differ significantly between different SESs or different numbers of iterations ($P > 0.05$). It was significantly better for normalization factors of 0.0005 and 0.001 as compared with a normalization factor of 0.002 ($P = 0.006$ and $P = 0.012$) or higher.

Multivariate regression analyses revealed that the parameters pulse sequence ($\beta = -0.148$, $P = 0.027$), iterations ($\beta = -0.311$, $P < 0.001$), and normalization factor ($\beta = 0.439$, $P < 0.001$) were significant independent influence factors with effects on blurring of the image. Soft tissue contrast was independently influenced by all parameters: pulse sequence ($\beta = 0.230$, $P < 0.001$), SESs ($\beta = -0.332$, $P < 0.001$), iterations ($\beta = 0.179$, $P = 0.004$), and normalization factor ($\beta = 0.389$, $P < 0.001$). Distortion of soft tissue was influenced by pulse sequence ($\beta = 0.547$, $P < 0.001$) and normalization factor ($\beta = 0.483$, $P < 0.001$). Pulse sequence ($\beta = 0.603$, $P < 0.001$) and normalization factor ($\beta = 0.476$, $P < 0.001$) were also identified to influence overall image quality independently.

Overall best soft tissue image quality was found for STIR and T1-w images with 19 SESs, 10 iterations, and a normalization factor of 0.001, and for T2-w images with 11 SESs, 10 iterations, and a normalization factor of 0.0005.

SNR and CNR Measurements

The results of the SNR analysis are given in the Supplementary Material S3, Supplemental Digital Content 3, http://links.lww.com/RLI/A397. Partial spearman correlations revealed significant correlations between SESs ($R = 0.30$, $P < 0.001$), iterations ($R = 0.28$, $P < 0.001$), and normalization factor ($R = 0.45$, $P = <0.001$) with $SNR_{agarose}$. There was a significant difference in $SNR_{agarose}$ between CS-SEMAC images with 19 SESs and 27 SESs (mean ± SEM, 137 ± 7 vs 181 ± 13, $P = 0.003$) but not between 11 SESs and 19 SESs (120 ± 7 vs 137 ± 7, $P = 0.087$). $SNR_{agarose}$ increased significantly from

TABLE 1. CS-SEMAC: Influence of SESs and Pulse Sequences on Different Parameters

Phantom Scans	**Mean ± SD**			**Mean Difference ± SEM (95% CI) *P***		
A	**11 SESs**	**19 SESs**	**27 SESs**	**11 vs 19 SESs**		**19 vs 27 SESs**
In-plane distortion	2.6 ± 0.9	1.7 ± 0.7	1.5 ± 0.5	0.9 ± 0.1 (0.6, 1.2); $P < 0.001$		0.2 ± 0.1 (0.0, 0.4); $P = 0.024$
Ripple artifacts	2.8 ± 0.7	3.1 ± 0.8	3.4 ± 0.7	−0.3 ± 0.1 (−0.5, −0.0); $P = 0.025$		−0.3 ± 0.1 (−0.6, −0.1); $P = 0.007$
Overall artifacts	2.8 ± 1.0	1.8 ± 0.8	1.9 ± 0.8	1.0 ± 0.1 (0.7, 1.3); $P < 0.001$		−0.1 ± 0.1 (−0.3, 0.2); $P = 0.678$
B	**STIR**	**T1-w**	**T2-w**	**STIR vs T1-w**	**STIR vs T2-w**	**T1-w vs T2-w**
In-plane distortion	2.0 ± 0.8	1.4 ± 0.7	2.3 ± 1.0	0.6 ± 0.1 (0.3, 0.8); $P < 0.001$	−0.3 ± 0.1 (−0.5, 0.0); $P = 0.079$	−0.8 ± 0.1 (−1.1, −0.6); $P < 0.001$
Ripple artifacts	3.2 ± 0.8	2.9 ± 0.7	3.1 ± 0.8	0.3 ± 0.1 (0.0, 0.5); $P = 0.025$	0.1 ± 0.1 (−0.2, 0.3); $P = 0.603$	−0.0 ± 0.1 (−0.4, 0.0); $P = 0.100$
Overall artifacts	2.4 ± 0.9	1.8 ± 0.8	2.3 ± 1.0	0.7 ± 0.1 (0.4, 0.9); $P < 0.001$	0.1 ± 0.2 (−0.2, 0.5); $P = 0.366$	−0.5 ± 0.2 (−0.8, −0.2); $P = 0.001$
Clinical Scans	**Mean ± SD**			**Mean Difference ± SEM (95% CI) *P***		
C	**11 SESs**	**19 SESs**		**11 vs 19 SESs**		
Blurring	3.0 ± 1.0	3.1 ± 0.8		−0.1 ± 0.1 (−0.4, 0.1); $P = 0.354$		
Soft tissue contrast	4.2 ± 0.9	3.5 ± 0.9		0.7 ± 0.1 (0.5, 1.0); $P < 0.001$		
Distortion of soft tissue	3.4 ± 1.4	3.0 ± 1.2		0.4 ± 0.2 (0.0, 0.8); $P = 0.034$		
Overall image quality	3.5 ± 1.4	3.2 ± 1.3		0.4 ± 0.2 (−0.0, 0.8); $P = 0.063$		
D	**STIR**	**T1-w**	**T2-w**	**STIR vs T1-w**	**STIR vs T2-w**	**T1-w vs T2-w**
Blurring	3.0 ± 0.8	3.5 ± 0.7	2.8 ± 0.8	−0.5 ± 0.2 (−0.8, −0.1); $P = 0.014$	0.2 ± 0.1 (0.1, 0.5); $P = 0.110$	0.7 ± 0.2 (0.4, 1.0); $P < 0.001$
Soft tissue contrast	3.3 ± 0.7	4.2 ± 0.7	4.0 ± 1.2	−1.0 ± 0.1 (−1.2, −0.7); $P < 0.001$	−0.7 ± 0.2 (−1.1, −0.4); $P < 0.001$	0.2 ± 0.2 (−0.1, 0.6); $P = 0.229$
Distortion of soft tissue	2.8 ± 0.4	3.8 ± 1.2	3.8 ± 1.1	−1.9 ± 0.2 (−2.3, −1.6); $P < 0.001$	−1.9 ± 0.2 (−2.2, −1.6); $P < 0.001$	0.0 ± 0.2 (−0.4, 0.4); $P = 0.902$
Overall image quality	1.9 ± 0.6	3.9 ± 1.1	4.0 ± 1.0	−2.0 ± 0.2 (−2.3, −1.6); $P < 0.001$	−2.1 ± 0.2 (−2.4, −1.8); $P < 0.001$	−0.1 ± 0.2 (−0.5, 0.3); $P = 0.521$

Mean semiquantitative scores ± standard deviation (SD) and mean differences ± standard error of the mean (SEM), lower and upper 95% confidence interval (CI) and *P* values are provided for parameters that describe metal artifact reduction on phantom scans (A and B), and for parameters that describe soft tissue appearance on clinical scans (C and D). $P < 0.05$ is considered statistically significant. Of note, there were no through-plane artifacts detected on any of the reconstructed images; ripple artifacts were only seen on MRI scans of the phantom.

TABLE 2. CS-SEMAC: Influence of Iterations and Normalization Factor on Different Parameters

Phantom Scans	Mean ± SD					Mean Difference ± SEM (95% CI) *P*	
A Iterations	**5**	**10**	**20**	**30**	**50**	**5 vs 20**	**20 vs 50**
In-plane distortion	2.6 ± 0.8	2.2 ± 0.9	1.7 ± 0.8; $P = 0.004$	1.5 ± 0.7	1.5 ± 0.7	0.9 ± 0.2 (0.6, 1.2); $P < 0.001$	0.2 ± 0.2 (−0.1, 0.5); $P = 0.151$
Ripple artifacts	2.1 ± 9.3	2.7 ± 9.5; $P < 0.001$	3.3 ± 0.5; $P < 0.001$	3.7 ± 0.5; $P = 0.001$	3.7 ± 0.5	−1.2 ± 0.1 (−1.4, −1.1); $P < 0.001$	−0.3 ± 0.1 (−0.5, 0.1); $P = 0.001$
Overall artifacts	3.1 ± 0.7	2.6 ± 0.7; $P = 0.003$	1.8 ± 0.9; $P < 0.001$	1.6 ± 0.8	1.6 ± 0.8	1.3 ± 0.2 (0.9, 1.6); $P < 0.001$	0.2 ± 0.2 (−0.1, 0.6); $P = 0.244$
B Normalization factor	**0.0005**	**0.001**	**0.002**	**0.003**	**0.005**	**0.0005 vs 0.002**	**0.002 vs 0.005**
In-plane distortion	1.7 ± 0.9	1.7 ± 0.9	1.8 ± 0.9	2.0 ± 0.9	2.3 ± 0.8	−0.1 ± 0.2 (−0.5, 0.3); $P = 0.639$	−0.5 ± 0.2 (−0.8, −0.1); $P = 0.011$
Ripple artifacts	3.1 ± 0.8	3.1 ± 0.8	3.1 ± 0.8	3.1 ± 0.8	3.1 ± 0.8	0.0 ± 0.2 (−0.3, 0.3); $P = 1.000$	0.0 ± 0.2 (−0.3, 0.3); $P = 1.0$
Overall artifacts	2.0 ± 1.0	1.9 ± 1.0	1.9 ± 1.0	2.3 ± 0.9	2.6 ± 0.7	0.1 ± 0.2 (−0.3, 0.5); $P = 0.680$	−0.7 ± 0.2 (−1.1, −0.4); $P < 0.001$
Clinical Scans	**Mean ± SD**					**Mean Difference ± SEM (95% CI) *P***	
C Iterations	**5**	**10**	**20**	**30**	**50**	**5 vs 20**	**20 vs 50**
Blurring	3.6 ± 0.8	3.2 ± 0.8; $P = 0.046$	2.9 ± 0.9	2.8 ± 0.9	2.8 ± 0.9	0.8 ± 0.2 (0.4, 1.2); $P < 0.001$	0.1 ± 0.2 (−0.3, 0.5); $P = 0.678$
Soft tissue contrast	3.6 ± 1.0	3.6 ± 1.2	4.0 ± 0.9	4.0 ± 1.0	4.1 ± 0.9	−0.4 ± 0.2 (−0.9, 0.1); $P = 0.094$	−0.1 ± 0.2 (−0.5, 0.4); $P = 0.781$
Distortion of soft tissue	3.5 ± 1.2	3.0 ± 1.4	2.9 ± 1.4	3.2 ± 1.3	3.3 ± 1.3	0.6 ± 0.3 (−0.1, 1.2); $P = 0.080$	−0.4 ± 0.3 (−1.0, 0.3); $P = 0.234$
Overall image quality	3.5 ± 1.3	3.1 ± 1.4	3.2 ± 1.5	3.5 ± 1.2	3.6 ± 1.2	0.2 ± 0.3 (−0.4, 0.9); $P = 0.474$	−0.3 ± 0.3 (−1.0, 0.3); $P = 0.322$
D Normalization Factor	**0.0005**	**0.001**	**0.002**	**0.003**	**0.005**	**0.0005 vs 0.002**	**0.002 vs 0.005**
Blurring	2.9 ± 0.8	2.5 ± 0.7; $P = 0.038$	2.8 ± 0.7; $P = 0.047$	3.3 ± 0.8; $P = 0.018$	3.7 ± 1.0	0.0 ± 0.2 (−0.3, 0.4); $P = 0.841$	−0.9 ± 0.2 (−1.3, 0.4); $P < 0.001$
Soft tissue contrast	3.5 ± 0.8	3.2 ± 1.0	3.7 ± 1.0	4.3 ± 0.9; $P = 0.006$	4.4 ± 0.8	−0.2 ± 0.2 (−0.7, 0.2); $P = 0.271$	−0.7 ± 0.2 (−1.1, −0.3); $P = 0.002$
Distortion of soft tissue	2.3 ± 0.8	2.3 ± 0.7	3.1 ± 1.0; $P < 0.001$	4.0 ± 1.3; $P = 0.002$	4.0 ± 1.3	−0.8 ± 0.2 (−1.2, −0.3); $P = 0.001$	−0.9 ± 0.3 (−1.5, −0.4); $P = 0.002$
Overall image quality	2.5 ± 0.9	2.5 ± 1.1	3.2 ± 1.1; $P = 0.012$	4.1 ± 1.3; $P = 0.005$	4.3 ± 1.2	−0.7 ± 0.2 (−1.2, −0.2); $P = 0.006$	−1.0 ± 0.3 (−1.6, −0.5); $P < 0.001$

Mean semiquantitative scores ± standard deviation (SD) and mean differences ± standard error of the mean (SEM), lower and upper 95% confidence interval (CI) and *P* values are provided for parameters that describe metal artifact reduction on phantom scans (A and B), and for parameters that describe soft tissue appearance on clinical scans (C and D). $P < 0.05$ is considered statistically significant. If differences between 2 consecutive means were significant, *P* values are given behind the mean of the higher number of iterations/normalization factor, respectively. Of note, there were no through-plane artifacts detected on any of the reconstructed images; ripple artifacts were only seen on MRI scans of the phantom.

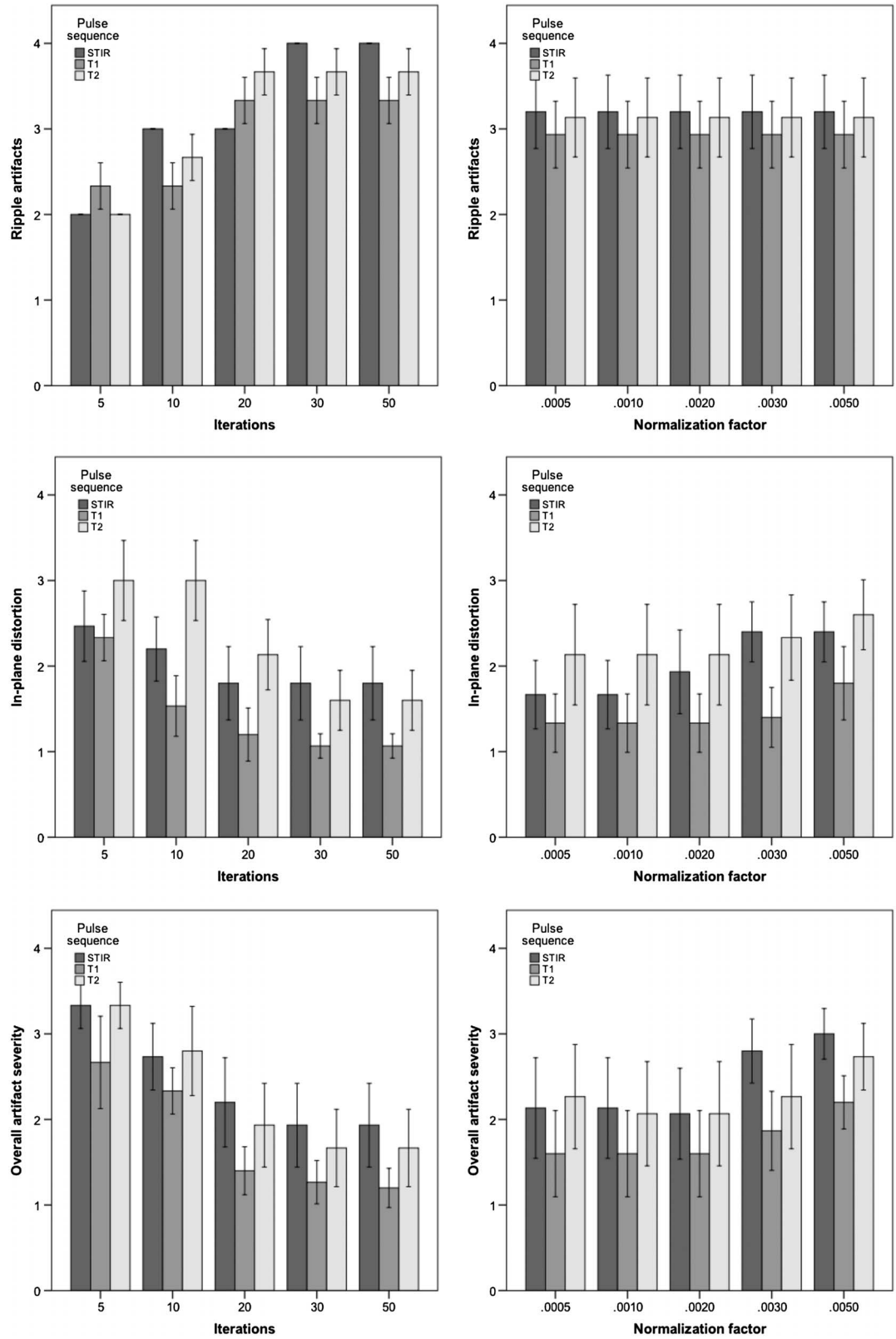

FIGURE 2. CS-SEMAC: Artifact scores (1–5, best–worst) for varying numbers of iterations (left column) and varying normalization factors (right column). Scores are provided for severity of ripple artifacts, in-plane distortion, and overall artifacts for each pulse sequence (short tau inversion recovery [STIR], T1-weighted [T1], and T2-weighted [T2]). Error bars represent 95% confidence intervals.

5 iterations to 10 iterations (100 ± 7 vs 130 ± 9; $P = 0.010$) and showed a statistical trend for a significance between 10 and 20 iterations (130 ± 9 vs 161 ± 14, $P = 0.074$); with more iterations, there was no further significant increase. $SNR_{agarose}$ increased with increasing normalization factors. The differences were significant for the steps 0.0005 to 0.001 (104 ± 6 vs 127 ± 8, $P = 0.031$) and 0.003 to 0.005 (157 ± 10 vs 211 ± 18, $P = 0.011$).

With respect to clinical MRI scans, SNR_{muscle} correlated significantly with SESs ($R = -0.17$, $P = 0.042$), iterations ($R = 0.17$, $P = 0.036$), and normalization factor ($R = 0.43$, $P < 0.001$). SNR_{fat} correlated significantly with iterations ($R = 0.19$, $P = 0.022$) and with normalization factor ($R = 0.52$, $P < 0.001$) but not with SESs ($R = -0.08$, $P = 0.363$). SNR_{fluid} correlated significantly with normalization factor ($R = 0.45$, $P < 0.001$) but not with SESs ($R = -0.02$, $P = 0.784$) or iterations ($R = 0.15$, $P = 0.072$). The CNRs of muscle versus fat correlated significantly with iterations ($R = 0.19$, $P = 0.024$) and normalization factor ($R = 0.52$, $P < 0.001$). The CNRs of fluid versus muscle only correlated significantly with normalization factor ($R = -0.28$, $P = 0.001$).

DISCUSSION

This study determined the optimal parameters for advanced acquisition and reconstruction algorithms during postprocessing of CS-SEMAC sequences for metal artifact reduced 1.5 T MRI of patients with THA. Although an excellent reduction of metal artifacts was achieved with all CS-SEMAC sequences that were acquired, the parameters determined in this study allow to reduce the well-known artifacts including those induced by the CS-SEMAC techniques and to optimize the duration of the image acquisition. The findings underline that not only the development of new metal artifact reduction techniques is important, but that optimization of scan protocol parameters is essential to guarantee an optimal image quality in patients with metal implants. Overall best soft tissue image quality was found for STIR and T1-w images with 19 SESs, 10 iterations, and a normalization factor of 0.001, and for T2-w images with 11 SESs, 10 iterations, and a normalization factor of 0.0005.

The prevalence of orthopedic metal implants is continuously rising. The most frequently performed joint replacement is THA.[9] During the postoperative course, some patients experience complications that involve the implant and the surrounding soft tissues and need further evaluation via MRI.[7] Conventional MARS sequences include optimized MR parameters such as high-bandwidth, small voxel size, short echo times, and so on.[21] New specialized MARS techniques include VAT, multiacquisition variable-resonance image combination, and SEMAC.[3,5–7,9,22–33] They allow a more accurate diagnosis with implications on treatment strategies. SEMAC reduces through-plane distortions via pseudo-3D acquisitions. It corrects for signal that is excited in wrong slice positions.[1,5,26,34] Advanced acceleration techniques such as partial Fourier, undersampling, and parallel imaging as well as advanced, postprocessing image reconstruction algorithms with iterative reconstruction are currently being combined with SEMAC techniques.[1,11] Those compressed sensing techniques in combination with SEMAC techniques (CS-SEMAC) allow to use SEMAC sequences with constant artifact reduction and image quality in clinically feasible acquisition times.[10–13] Worters et al[11] showed in 13 subjects with spinal implants that using compressed sensing techniques result in no loss of diagnostic quality. For knee arthroplasties and THA, Fritz et al[10,13] demonstrated that CS-SEMAC sequences allow a time-neutral use of SEMAC techniques with better image quality than high-bandwidth sequences and quality similar to lengthier SEMAC pulse sequences. CS-SEMAC improved the diagnosis of pathologies adjacent to total ankle arthroplasties resulting in a positive effect on patient management.[17]

Several studies used similar experimental setups for evaluation of MARS sequences.[35] In the present study, an agarose/gadolinium mixture was used to achieve an intermediate to high T2 signal as well as an intermediate to high T1 signal for improved visualization of artifacts on all pulse sequences. On phantom scans, the overall extent of artifacts was small in all acquired CS-SEMAC sequences, which is consistent with previous observations.[10,13,17,36] Residual ripple artifacts were already described as typical artifacts induced by SEMAC sequences.[10,19] We could demonstrate that ripple artifacts increased with more SESs and iterations. Ripple artifacts were not visible on clinical MRI scans, from which we conclude that they are of minor importance in the context of clinical CS-SEMAC MARS imaging of THA.

The parameters evaluated in the present study (SESs, iterations, and normalization factor) may be adjusted by the MR technician directly at the parameter display of the MR computer console. SESs are the number of adjacent slices whose signal is assessed for artifact reduction during readout of SEMAC sequences for one specific slice.[5] The required coverage is dependent on the implant material and the extent of the resulting field inhomogeneities.[1,6] The current main issues of SEMAC sequences are very long scan times that increase with increasing numbers of SESs. Thus, for metals such as stainless steel that cause large artifacts and that require many SESs, techniques that reduce the scan time may be most helpful. None of the available CS-SEMAC studies varied the number of SESs or other parameters to optimize those advanced image acquisition and reconstruction techniques.[10,11] CS-SEMAC sequences are usually provided by the manufacturer with 19 SESs. In test scans of the phantom, it was found that a maximum of 27 SESs was technically feasible. Standard SEMAC sequences (without CS) had been frequently acquired with 6 to 12 SESs.[7–9,36–38] Therefore 11, 19, and 27 SESs were assessed in this study. More SESs were associated with higher SNR, reduced metal artifacts, and improved imaged quality, but images showed more severe ripple artifacts and had longer acquisition and reconstruction times; 19 SESs were identified to be sufficient for optimal artifact reduction. Twenty-seven SESs exceeded computer and processor power. Although during the time of image reconstruction other pulse sequences of the same patient may be acquired, no other patient may be scanned on the same console during reconstruction time. The issue of reconstruction time, computation power, and processor speed has not been discussed so far.[10,11,13,17]

More iterations were associated with reduced metal artifacts and reduced blurring, but also with more severe ripple artifacts and longer reconstruction times. None of the parameters improved significantly with application of 30 or 50 iterations as compared with 20 iterations. In clinical scans, 10 iterations resulted in sufficient image quality for all assessed sequences. Previously, based on initial empirical experience, 15,[17] 19,[4] and 20[10,13] iterations were applied for imaging of ankle, hip, and knee replacements. These numbers of iterations seem reasonable, whereas 30 iterations are more time-consuming without any profit.[10,13,17]

By exploration of missing image information, smoothening, and contrast enhancement, a higher normalization factor (regularization parameter) causes an artificial appearance of the soft tissue on CS-SEMAC images and the delineation of anatomical structures decreases.[1] The optimal normalization factor was 0.001 for STIR and T1-w sequences and 0.0005 for T2-w sequences. Those studies that previously reported the normalization factor used a wide range of 0.0005,[17] 0.0025,[10] 0.005, or 0.008, based on initial empirical experience.[13] Although a normalization factor of 0.0025 may still seem reasonable (in our study most parameters got worse with a normalization factor of 0.003), higher normalization factors cause soft tissue distortion and artificial image appearance. Fritz et al[13] stated that optimization of iterations and normalization factors are required, which our study provides both in phantom scans and clinical scans.

The study has limitations. First, a structured analysis was only performed of coronal images both in the phantom and in the patients because this is the main plane for MRI of THA and other joint replacements. For the sagittal and for the transverse plane, only exemplary phantom scans were performed in preparation of this study, which demonstrated feasibility and transferability of the results to the other planes

(data not shown). Second, a number of 19 SESs proved to be sufficient for a robust and clinically applicable artifact reduction as well as for optimal image quality; a further increase of SESs is not necessary. Whether 13, 15, or 17 SESs would also be sufficient for optimal image quality may not be determined by the present study. Last, artifact reduction was assessed in one phantom. Following, it can only be assumed that with other implants and implant materials, optimal artifact reduction is achieved with the same parameters.

In conclusion, optimized advanced acceleration and reconstruction algorithms of CS-SEMAC have been identified to reduce metal artifacts in patients with THA enabling imaging with clinically feasible acquisition and reconstruction times.

REFERENCES

1. Jungmann PM, Agten CA, Pfirrmann CW, et al. Advances in MRI around metal. *J Magn Reson Imaging*. 2017;46:972–991.
2. Fritz J, Lurie B, Miller TT, et al. MR imaging of hip arthroplasty implants. *Radiographics*. 2014;34:E106–E132.
3. Runge VM. Current technological advances in magnetic resonance with critical impact for clinical diagnosis and therapy. *Invest Radiol*. 2013;48:869–877.
4. Kumar NM, de Cesar Netto C, Schon LC, et al. Metal artifact reduction magnetic resonance imaging around arthroplasty implants: the negative effect of long echo trains on the implant-related artifact. *Invest Radiol*. 2017;52:310–316.
5. Lu W, Pauly KB, Gold GE, et al. SEMAC: slice encoding for metal artifact correction in MRI. *Magn Reson Med*. 2009;62:66–76.
6. Filli L, Jud L, Luechinger R, et al. Material-dependent implant artifact reduction using SEMAC-VAT and MAVRIC: a prospective MRI phantom study. *Invest Radiol*. 2017;52:381–387.
7. Jungmann PM, Ganter C, Schaeffeler CJ, et al. View-angle tilting and slice-encoding metal artifact correction for artifact reduction in MRI: experimental sequence optimization for orthopaedic tumor endoprostheses and clinical application. *PLoS One*. 2015;10:e0124922.
8. Agten CA, Del Grande F, Fucentese SF, et al. Unicompartmental knee arthroplasty MRI: impact of slice-encoding for metal artefact correction MRI on image quality, findings and therapy decision. *Eur Radiol*. 2015;25:2184–2193.
9. Sutter R, Ulbrich EJ, Jellus V, et al. Reduction of metal artifacts in patients with total hip arthroplasty with slice-encoding metal artifact correction and view-angle tilting MR imaging. *Radiology*. 2012;265:204–214.
10. Fritz J, Fritz B, Thawait GK, et al. Advanced metal artifact reduction MRI of metal-on-metal hip resurfacing arthroplasty implants: compressed sensing acceleration enables the time-neutral use of SEMAC. *Skeletal Radiol*. 2016;45:1345–1356.
11. Worters PW, Sung K, Stevens KJ, et al. Compressed-sensing multispectral imaging of the postoperative spine. *J Magn Reson Imaging*. 2013;37:243–248.
12. Lustig M, Donoho D, Pauly JM. Sparse MRI: the application of compressed sensing for rapid MR imaging. *Magn Reson Med*. 2007;58:1182–1195.
13. Fritz J, Ahlawat S, Demehri S, et al. Compressed sensing SEMAC: 8-fold accelerated high resolution metal artifact reduction MRI of cobalt-chromium knee arthroplasty implants. *Invest Radiol*. 2016;51:666–676.
14. Vreemann S, Rodriguez-Ruiz A, Nickel D, et al. Compressed sensing for breast MRI: resolving the trade-off between spatial and temporal resolution. *Invest Radiol*. 2017;52:574–582.
15. Yang AC, Kretzler M, Sudarski S, et al. Sparse reconstruction techniques in magnetic resonance imaging: methods, applications, and challenges to clinical adoption. *Invest Radiol*. 2016;51:349–364.
16. Yoon JH, Lee SM, Kang HJ, et al. Clinical feasibility of 3-dimensional magnetic resonance cholangiopancreatography using compressed sensing: comparison of image quality and diagnostic performance. *Invest Radiol*. 2017;52:612–619.
17. de Cesar Netto C, Fonseca LF, Fritz B, et al. Metal artifact reduction MRI of total ankle arthroplasty implants. *Eur Radiol*. 2017.
18. Kato H, Kuroda M, Yoshimura K, et al. Composition of MRI phantom equivalent to human tissues. *Med Phys*. 2005;32:3199–3208.
19. den Harder JC, van Yperen GH, Blume UA, et al. Ripple artifact reduction using slice overlap in slice encoding for metal artifact correction. *Magn Reson Med*. 2015;73:318–324.
20. Firbank MJ, Harrison RM, Williams ED, et al. Quality assurance for MRI: practical experience. *Br J Radiol*. 2000;73:376–383.
21. Ariyanayagam T, Malcolm PN, Toms AP. Advances in metal artifact reduction techniques for periprosthetic soft tissue imaging. *Semin Musculoskelet Radiol*. 2015;19:328–334.
22. Cho ZH, Kim DJ, Kim YK. Total inhomogeneity correction including chemical shifts and susceptibility by view angle tilting. *Med Phys*. 1988;15:7–11.
23. Choi SJ, Koch KM, Hargreaves BA, et al. Metal artifact reduction with MAVRIC SL at 3-T MRI in patients with hip arthroplasty. *AJR Am J Roentgenol*. 2015;204:140–147.
24. Koch KM, Brau AC, Chen W, et al. Imaging near metal with a MAVRIC-SEMAC hybrid. *Magn Reson Med*. 2011;65:71–82.
25. Koch KM, Hargreaves BA, Pauly KB, et al. Magnetic resonance imaging near metal implants. *J Magn Reson Imaging*. 2010;32:773–787.
26. Ai T, Padua A, Goerner F, et al. SEMAC-VAT and MSVAT-SPACE sequence strategies for metal artifact reduction in 1.5T magnetic resonance imaging. *Invest Radiol*. 2012;47:267–276.
27. Liebl H, Heilmeier U, Lee S, et al. In vitro assessment of knee MRI in the presence of metal implants comparing MAVRIC-SL and conventional fast spin echo sequences at 1.5 and 3 T field strength. *J Magn Reson Imaging*. 2015;41:1291–1299.
28. Lee YH, Lim D, Kim E, et al. Usefulness of slice encoding for metal artifact correction (SEMAC) for reducing metallic artifacts in 3-T MRI. *Magn Reson Imaging*. 2013;31:703–706.
29. Sutter R, Hodek R, Fucentese SF, et al. Total knee arthroplasty MRI featuring slice-encoding for metal artifact correction: reduction of artifacts for STIR and proton density-weighted sequences. *AJR Am J Roentgenol*. 2013;201:1315–1324.
30. Hargreaves BA, Chen W, Lu W, et al. Accelerated slice encoding for metal artifact correction. *J Magn Reson Imaging*. 2010;31:987–996.
31. Butts K, Pauly JM, Gold GE. Reduction of blurring in view angle tilting MRI. *Magn Reson Med*. 2005;53:418–424.
32. Hayter CL, Koff MF, Shah P, et al. MRI after arthroplasty: comparison of MAVRIC and conventional fast spin-echo techniques. *AJR Am J Roentgenol*. 2011;197:W405–W411.
33. Farshad-Amacker NA, Koff MF, Dyke JP, et al. Assessment of osteonecrosis in the presence of instrumentation for femoral neck fracture using contrast-enhanced MAVRIC sequence. *HSS J*. 2016;12:51–58.
34. Lu W, Pauly KB, Gold GE, et al. Slice encoding for metal artifact correction with noise reduction. *Magn Reson Med*. 2011;65:1352–1357.
35. van Gorp JS, Nizak R, Bouwman JG, et al. Multispectral 3D phase-encoded turbo spin-echo for imaging near metal: limitations and possibilities demonstrated by simulations and phantom experiments. *Magn Reson Imaging*. 2017;39:31–43.
36. Mansson S, Muller GM, Wellman F, et al. Phantom based qualitative and quantitative evaluation of artifacts in MR images of metallic hip prostheses. *Phys Med*. 2015;31:173–178.
37. Deligianni X, Bieri O, Elke R, et al. Optimization of scan time in MRI for total hip prostheses: SEMAC tailoring for prosthetic implants containing different types of metals. *Rofo*. 2015;187:1116–1122.
38. Lee YH, Hahn S, Kim E, et al. Fat-suppressed MR imaging of the spine for metal artifact reduction at 3T: comparison of STIR and slice encoding for metal artifact correction fat-suppressed T2-weighted images. *Magn Reson Med Sci*. 2016;15:371–378.